Mem. Fac. Eng., Kyoto Univ., Vol. 55, No. 2 (1993)

A Six-Axis Force Sensor with Three-Dimensional Cross-Shape Structure

By

Tsuneo YOSHIKAWA* and Taizou MIYAZAKI†

(Received November 5, 1992)

Abstract

A new six-axis force sensor is described. It has three pairs of elastic elements that are orthogonal to each other and cross at the center of the sensor. Each elastic element consists of a pair of thin parallel plates which is called a parallel plate structure. From the outputs of the strain gauges placed on the elastic elements, the six force components are obtained. This orthogonal structure, which is named the three-dimensional cross-shape structure, has the following merits. (1) The whole characteristic of the sensor is obtainable just by analyzing the force-strain relation of a pair of elastic elements on an axis, maing it simpler to design a sensor for a given specification. (2) The cross-coupling between the strain gauge outputs and the six force components can be made small. (3) It is easy to design a rigid sensor. A prototype sensor has been fabricated and it has ben shown that the measured characteristic coincides with the analysis based on the beam theory; the cross-coupling is rather small, and the force-strain characteristics in all force directions are uniform. A few design considerations are also given.

1. Introduction

Research is actively being done for the application of robotic manipulators to more sophisticated tasks such as assembly, polishing, deburring, etc. For these tasks it is desirable to control not only the position of a manipulator but also the force exerted by the end-effector on an object [1]–[6]. Force sensors, especially general six-axis force sensors, play a key role in the force control.

Many force sensors have been developed so far [7]–[13], and severar six-axis force sensors are commercially available [13], [10], [11]. However there are still several problems unsolved. First, not much analytical study has ben done because of the complexities of elastic elements and large cross-coupling among strain gauge outputs for each axial force element. Hence the design of a sensor for a given specification of forces and torques sems to have been heuristic and based on the

* Department of Mechanical Engineering.
† Student, Department of Precision Mechanics.
Presently with Hitachi, Ltd.

designer's experiences. As for the evaluation of designed sensors, several theoretical approaches have been proposed recently [14], [15]. The second problem is that many of the sensors need some data processing of the measured strain gauge outputs due to the cross-coupling. It is desirable to develop a sensor with less cross-coupling for easy application to on-line force control.

In this paper, we propose a new structure for six-axis force sensors which is easy to analyze and has a small cross-coupling in principle. To examine the validity of the new sensor structure, the analytical results are compared with the measurements of a prototype force sensor.

2. Force Sensor with Three-Dimensional Cross-Shape Structure

The conceptual structure of the proposed sensor is shown in Fig. 1. In the figure, the top and bottom plates mean the outer covers of the sensor where the force is applied. The six hatched squares are elastic elements where forces are detected through the strains. The other solid lines are structures which are so rigid that it's strain caused by any external force within the sensor specification is neglibly small. As the elastic element we adopt the parallel plate structure [9], [10] (abbreviated as PPS hereafter). By the pair of PPS on the the X axis we detect the force F_z in Z direction and the moment M_y on the Y axis. Similarly, with the other two pairs of PPS on the Y and X axes we detect other force

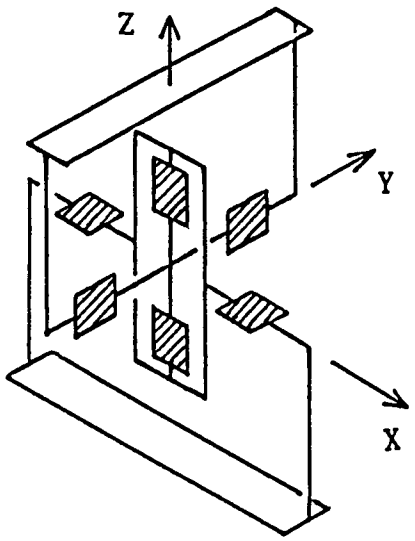

Fig. 1 Conceptual Structure of the Proposed Sensor.

components: F_X, M_Z, F_Y, and M_X. An example of the sensor design based on the above concept is given in Fig. 2. Fig. 2 (a) shows the overview. (b) and (c) show the two parts of the sensor, which are separated just for ease of understanding. They have the hatched parts in common. The pair of PPS (thin plates on the side of square holes) on the X axis is shown in (b) and the pairs of PPS on the Y and Z axes are shown in (c).

Sensors with the above-stated three-dimensional cross-shaped structure have the following merits.

1) The arrangement of the elastic elements is the same with respect to all three axies, and simple. Most of the existing sensors have a Z-axis structure different from the other two axes.

2) By designing the elastic elements on the X axis so that the strains by force components F_Z and M_y are much larger than those by other force components,

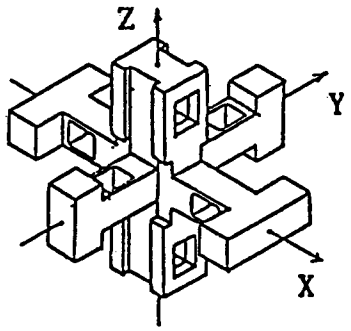

(a) Overview

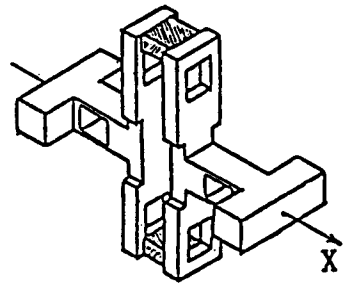

(b) PPS on X axis

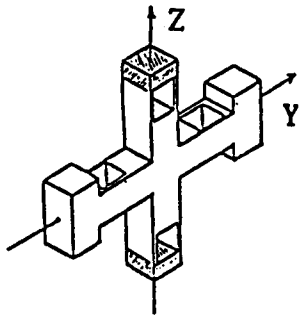

(c) PPS on Y and Z axes

Fig. 2 Structure of Sensor

and designing the other elastic elements in the same way, we can make the cross-coupling small. Thus there is a possibility of shortening the processing time of the measured data. The PPS is a good design from the viewpoint above. The design above will also lead to a highly rigid sensor.

3) Due to characteristic 1), all the properties of the sensor are easily derived from the properties of a pair of PPS on an axis, making it easy to design a sensor that matches a given specification.

Hence for the design of the sensor shown in Fig. 2, it is enough to formulate the relation between the force and strain of a pair of PPS on an axis. Although Tani et al. [9] have analyzed a PPS of the cantilever type, the case of a pair of PPS in a beam with both ends fixed has not been analyzed. This will be done in the following section.

3. Analysis of PPS

Fig. 3 shows a model of a pair of PPS. As shown in the figure, it is divided into three parts, i.e., the central block part, end block part, and plate part.

We assume that the central and end block parts are not deformed at all by the application of force, and that the plate parts can be modeled as cantilevers. Notation d means the distance from the center to the PPS, l is the length of the plate, t is the thickness of the plate, b is the width of the plate, h is the distance between the center lines of two plates, and h_b is the thickness of the central block part. Note that $h_b = h + b$.

The strain on the outer surface of the plate from force F and moment M applied on the center of the PPS model will be derived. We consider the three

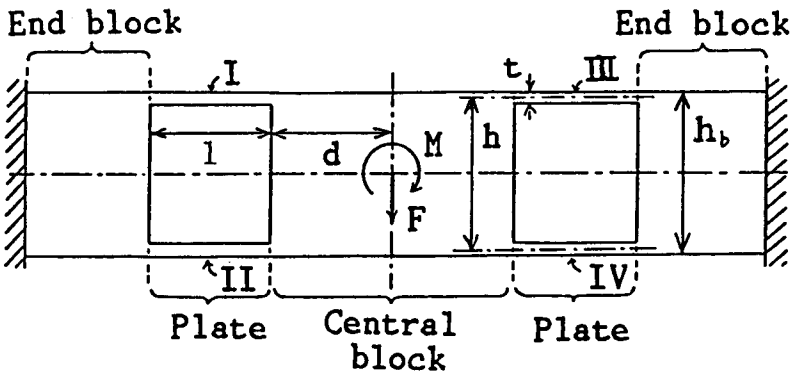

Fig. 3 Model of PPS

cases; 1) force F only, 2) moment M only, and 3) force F and moment M.

1) Case of Force F Only

When only a force F is applied on the center of the PPS model, the deflection, when exaggerated, is given by Fig. 4. From the above assumption, plate I can be regarded as a cantilever, as shown in Fig. 5. We define the coordinate frame $\xi-\eta$ as shown in the figure and assume that the strain is very small. Let the force and moment at the free end be f_1 and m_1. Then the bending moment $M_1(\xi)$ at position ξ is given by

$$M_1(\xi)=m_1-f_1(l-\xi) \tag{1}$$

Note that $M_1(\xi)$ is taken to be positive when it is a clockwise moment. Denoting the deflective curve as $\eta(\xi)$ and letting $\eta'(\xi)=d\eta(\xi)/d\xi$, $\eta''(\xi)=d^2\eta(\xi)/d\xi^2$, we have from Hook's law

$$\eta''(\xi)=-\frac{M_1(\xi)}{EI} \tag{2}$$

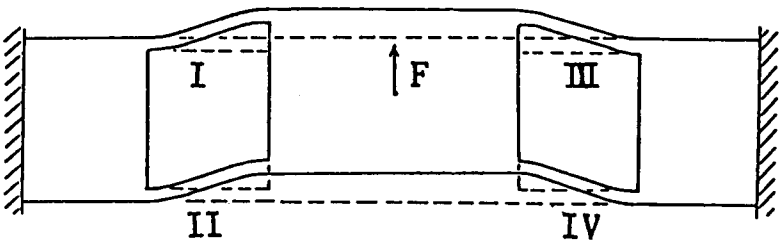

Fig. 4 Deformation by Force F

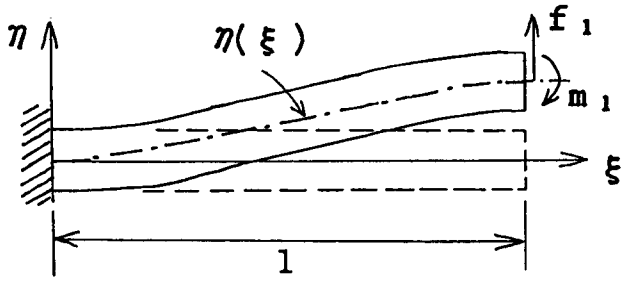

Fig. 5 Cantilever Model of Plate I.

where E is the modulus of elasticity and I is the second moment of area. In our case, $I=bt^3/12$. Integrating (2) under the boundary condition $\eta(0)=0$, $\eta'(0)=0$ yields

$$\eta'(\xi)=-\frac{1}{EI}\{(m_1-f_1l)\xi+\frac{1}{2}f_1\xi^2\} \tag{3}$$

$$\eta(\xi)=-\frac{1}{EI}\{\frac{1}{2}(m_1-f_1l)\xi^2+\frac{1}{6}f_1\xi^3\} \tag{4}$$

By the symmetry of the model and the assumption of no deformation of the central block, we have the following boundary condition at the free end:

$$\eta'(l)=0 \tag{5}$$

From (5) and (3) we have

$$m_1=\frac{f_1}{2}l \tag{6}$$

Considering the force balance of the central block, we have

$$f_1=\frac{F}{4} \tag{7}$$

Hence from (1), (6), (7)

$$M_1(\xi)=-\frac{1}{8}(2\xi-l)F \tag{8}$$

The strain $\varepsilon_{F1}(\xi)$ on the upper surface of plate I (and plate III) is given by

$$\varepsilon_{F1}(\xi)=\frac{M_1(\xi)}{EI}\cdot\frac{t}{2}=\frac{3}{4Ebt^2}(2\xi-l)F \tag{9}$$

Similarly the strain on the lower surface of plate II (and plate IV) is given by

$$\varepsilon_{F2}(\xi)=\frac{-3}{4Ebt^2}(2\xi-l)F \tag{10}$$

2) Case of Moment M Only

When only a moment M is applied on the center of the PPS model, due to the symmetry of plates I~IV, we can assume that the center does not deflect, that the deflections of plates I and IV are the same, and that those of plates II and III are the same as shown in Fig. 6. Therefore we introduce the unknown forces at the free ends of the plates as in Fig. 7. Here f_{1H} and f_{2H} are horizontal forces, f_{1V}, f_{2V} are vertical forces, and m_1 and m_2 are moments.

We first consider plate I, which can be regarded as a cantilever as shown in Fig. 8. Assuming that the vertical deflection due to f_{1H} is negligible, as in (1), (3) and (4), the bending moment $M_1(\xi)$ due to f_{1V} and m_1, and the deflection curve $\eta_1(\xi)$ satisfying $\eta_1(0)=0$, $\eta_1'(0)=0$ are given by

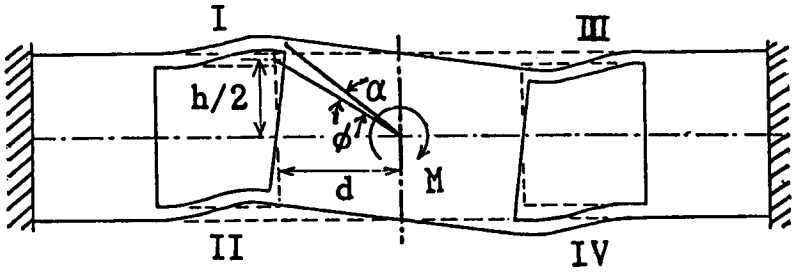

Fig. 6 Deformation by Moment M

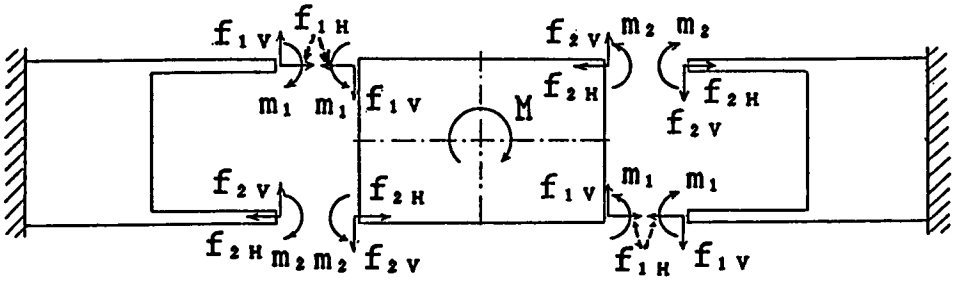

Fig. 7 Unknown Forces for the Case of Moment M Only

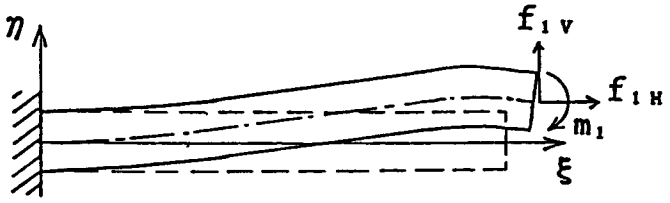

Fig. 8 Cantilever Model of Plate I

$$M_1(\xi)=m_1 f_{1V}(l-\xi) \tag{11}$$

$$\eta_1'(\xi)=-\frac{1}{EI}\{(m_1-f_{1V}l)\xi+\frac{1}{2}f_{1V}\xi^2 \tag{12}$$

$$\eta_1(\xi)=-\frac{1}{EI}\{\frac{1}{2}(m_1-f_{1V}l)\xi^2+\frac{1}{6}f_{1V}\xi^3\} \tag{13}$$

On the other hand, the horizontal deflection ξ_1 at the free end due to f_{1H} is given by

$$\xi_1=\frac{l}{Ebt}f_{1H} \tag{14}$$

Now we consider the boundary condition at the free end. If the central block part rotates by an infinitesimal angle α, the horizontal deflection ξ_1 and the vertical deflection $\eta_1(l)$ should satisfy

$$\xi_1=\alpha h/2 \tag{15}$$

$$\eta_1(l)=\alpha d \tag{16}$$

and the inclination at the free end should satisfy

$$\eta_1'(l)=-\alpha \tag{17}$$

Hence from (12), (13), (14) and the boundary conditions (15), (16), (17), we obtain

$$f_{1V}=\frac{3(l+2d)}{l(2l+3d)}m_1 \tag{18}$$

$$f_{1H}=\frac{3hl}{t^2(2l+3d)}m_1 \tag{19}$$

Similar argument holds for plate II. Defining the coordinates as shown in Fig. 9 and letting $\eta_2(\xi)$ be the deflection curve due to f_{2V} and m_2, and letting ξ_2 be the horizontal deflection of the free end due to f_{2H}, we obtain

$$\eta_2(\xi)=-\frac{1}{EI}\{\frac{1}{2}(m_2-f_{2V}l)\xi^2+\frac{1}{6}f_{2V}\xi^3\} \tag{20}$$

$$\xi_2=-\frac{l}{Ebt}f_{2H} \tag{21}$$

$$f_{2V}=\frac{3(l+2d)}{l(2l+3d)}m^2 \tag{22}$$

$$f_{2H}=\frac{3hl}{t^2(2l+3d)}m^2 \tag{23}$$

Since $\eta_1'(l)=\eta_2'(l)$ due to the assumption of non-deformation of the central block part, we have $m_1=m_2$ from (12), (20). Hence from (18), (19), (22), (23), we obtain $f_{1V}=f_{2V}$, $f_{1H}=f_{2H}$.

The equilibrium equation of moments acing on the central block part is

$$\begin{aligned}M&=h(f_{1H}+f_{2H})+2d(f_{1V}+f_{2V})+2(m_1+m_2)\\&=2hf_{1H}+4df_{1V}+4m_1\end{aligned} \tag{24}$$

Hence from (18), (19), (24)

$$m_1=\frac{t^2l(2l+3d)}{6h^2l^2+8t^2(3d^2+3dl+l^2)}M \tag{25}$$

Substituting (25) and (18) into (11) yields

$$M_1(\xi)=\frac{t^2l(l+3d)-3t^2(l+2d)\xi}{6h^2l^2+8t^2(3d^2+3dl+l^2)}M \tag{26}$$

The strain $\varepsilon_{M1}(\xi)$ on the upper surface of plate I (or the lower surface of plate IV) is given by the sum of the strains by $M_1(\xi)$ and f_{1H} as

$$\varepsilon_{M1}(\xi)=\frac{M_1(\xi)}{EI}\left(\frac{t}{2}\right)+\frac{f_{1H}}{Ebt} \tag{27}$$

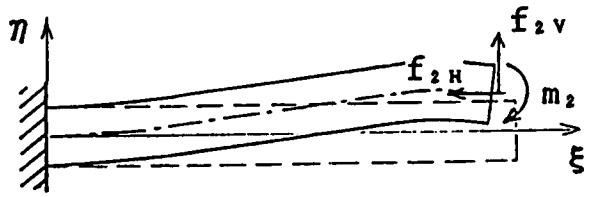

Fig. 9 Cantilever Model of Plate II

or

$$\varepsilon_{M1}(\xi)=\frac{3[hl^2-2tl(l+3d)+6t(2d+l)\xi]}{Ebt[6h^2l^2+8t^2(3d^2+3dl+l^2)]}M \tag{28}$$

Similarly the strain $\varepsilon_{M2}(\xi)$ on the lower surface of plate II (or the upper surface of plate III) is given by

$$\varepsilon_{M2}(\xi)=-\varepsilon_{M1}(\xi) \tag{29}$$

3) Case of Combination of Force F and Moment M

We assume that the deflections are small such that the strain $\varepsilon(\xi)$ for the case of combined F and M is given by the superposition of the cases of F only and M only. For plates I and IV, from (9), (10), and (28) we have

$$\varepsilon(\xi)=\frac{3}{4Ebt^2}\left[\left\{\frac{2thl^2-4t^2l(l+3d)+12t^2(2d+l)\xi}{3h^2l^2+4t^2(3d^2+3dl+l^2)}\right\}M\pm(2\xi-l)F\right] \tag{30}$$

where the sign $\pm$ takes $+$ for plate I, and $-$ for plate IV. Similarly, for plates II and III, we have

$$\varepsilon(\xi)=\frac{-3}{4Ebt^2}\left[\left\{\frac{2thl^2+4t^2l(l+3d)-12t^2(2d+l)\xi}{3h^2l^2+4t^2(3d^2+3dl+l^2)}\right\}M\pm(2\xi-l)F\right] \tag{31}$$

where the sign $\pm$ takes $+$ for plate II and $-$ for plate III.

The PPS structure was originally introduced as a structure which is easily deformed by forces normal to the plates but is hardly deformed by moments about an axis in the transversal direction of the plates. But the above analysis shows the possibility of measuring both forces and moments by a proper choice of dimensions of the PPS. Notice that the sensors developed by Hitachi Construction Machinery Co., Ltd. [10] and Fujitsu Laboratories, Ltd. [11] already exploit this fact. Hence the result of this section would be applicable to the analysis of these sensors.

4. Measurement of Strain Distribution

To examine whether equations (30) and (31) can be used for the analysis and design of sensors, the distribution of strain on the surfaces of plates are

measured for a prototype six-axis sensor with dimensions $b=10$ (mm), $d=15$ (mm), $h=9.4$ (mm), $l=8$ (mm), and $t=0.6$ (mm) (hence $h_b=10$ (mm)). Fig. 10 shows the prototype sensor. The three-dimensional cross-shaped structure and the top and bottom covers are connected by screws. Strain distributions of the PPS in the X and Y axes are measured using the strain gauges placed on the center line 2 mm apart as shown in Fig. 11. The length of each gauge is 1 mm.

Measurements are shown in Fig. 12 and 13. The strain distributions, drawn with solid lines, of the PPS in the Y axis, agree rather well for both F_Y and M_Z with the analytical distributions, drawn with broken lines, calculated from (30). However that of the PPS in the X axis for moment M_Y has some discrepancy with the analysis. This discrepancy would probably be caused by (A) deformation due to the lack of strength of the central part shown in Fig. 2 (b), or (B) by an insufficient constraint at the screw connections between the end blocks and the bottom cover. Figures 12 and 13 show that equations (30) and (31) can be used for the analysis and design of force sensors if we pay a little attention to the above two points (A) and (B). It can also be seen that the best place for placing the strain gauge is the boundary between the central block and the plate.

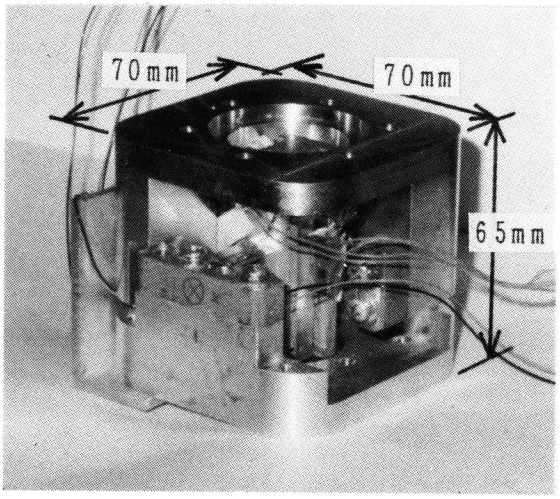

Fig. 10 Overview of Prototype Sensor

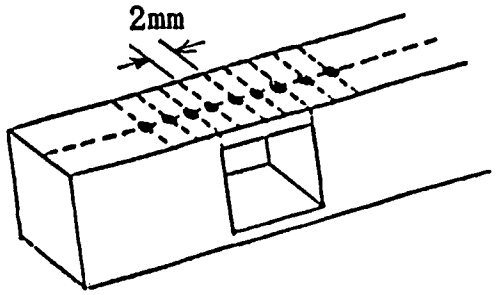

Fig. 11 Position of Strain Gauges for Measuring the Strain Distribution

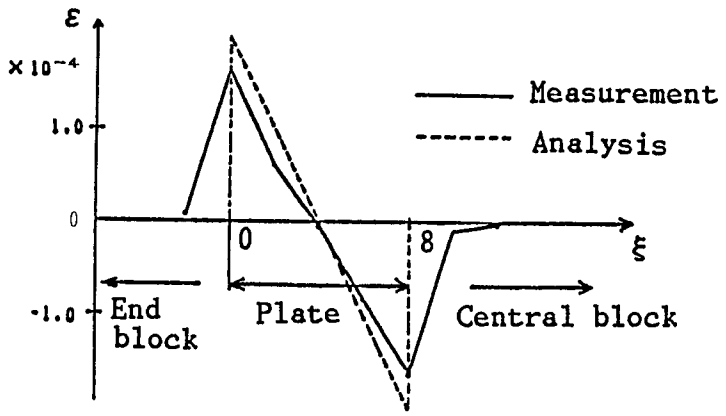

(a) $F_Z = -1.0$ kg

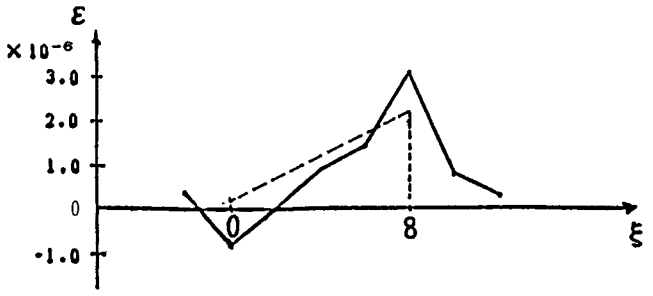

(b) $M_Y = 1.0$ kgf·mm

Fig. 12 Strain Distribution of PPS in X Axis

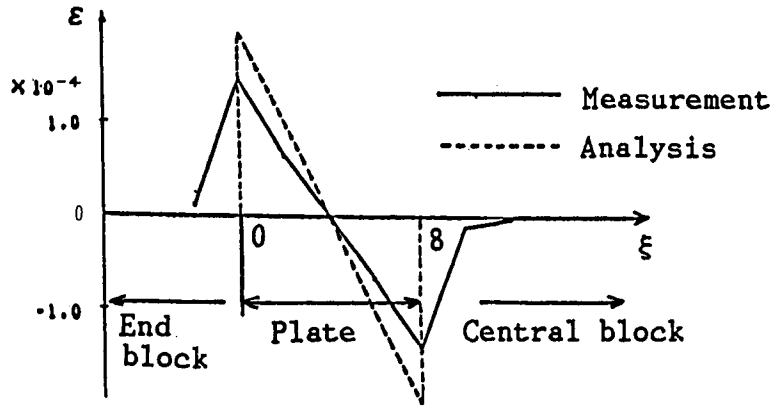

(a) $F_Y = -1.0$ kg

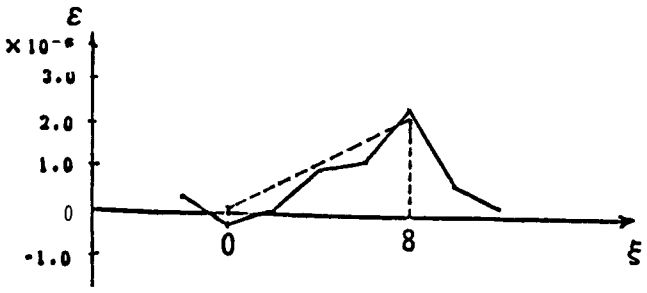

(b) $M_Z = 1.0$ kgf·mm

Fig. 13 Strain Distribution of PPS in Y Axis

5. Study of the Effect of End Block Constraint on Strain Distribution by Finite Element Method

It was observed in the previous section that the strain of the PPS on the X axis for moment M_Y is larger than that calculated by (30). In order to examine the effect of the end block constraint on the strain distribution, which was pointed out as a possible cause of this discrepancy, the distribution was calculated by the Finite Element Method (FEM) under different end block constraints. Fig. 14 shows complete constraint on both position and orientation of the end blocks, and Fig. 15 shows a weak constraint where the horizontal displacement and rotation of the end blocks are free. Broken lines in the figures are analytical distributions calculated by (30). From the figures it is seen that the response to force F does

not vary very much but that the strain for moment M is much larger in the case of weak constraint. From this fact, we can tell the following two points.

(1) If we want the ratio $R=|M/F|$ of force F and moment M, which give the same strain at $\xi=l$, to be large, it is important to make the end block constraints as complete as possible at the stage of design and fabrication.

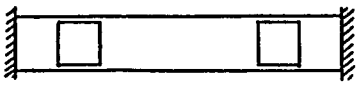

(a) Constraint

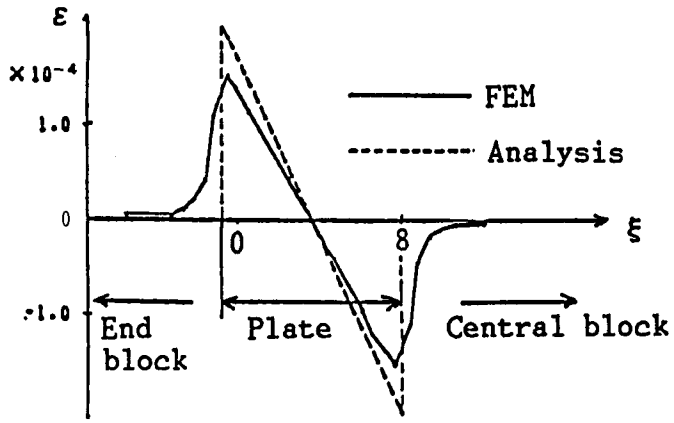

(b) $F=1.0$ kg

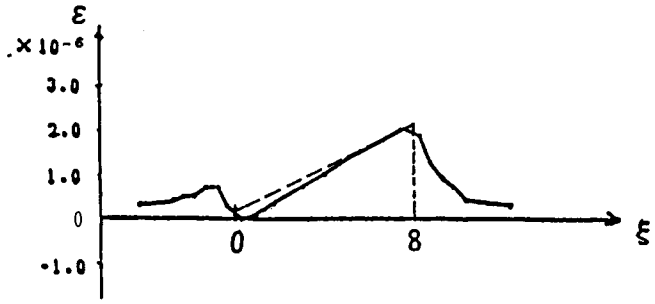

(c) $M=1.0$ kgf·mm

Fig. 14 Strain Distribution by FEM under Complete End-Block Constraint

(2) If we want the ratio R small, one approach is to design the end block constraint to be weak.

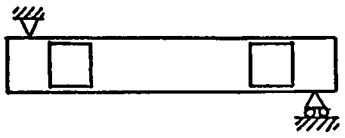

(a) Constraint

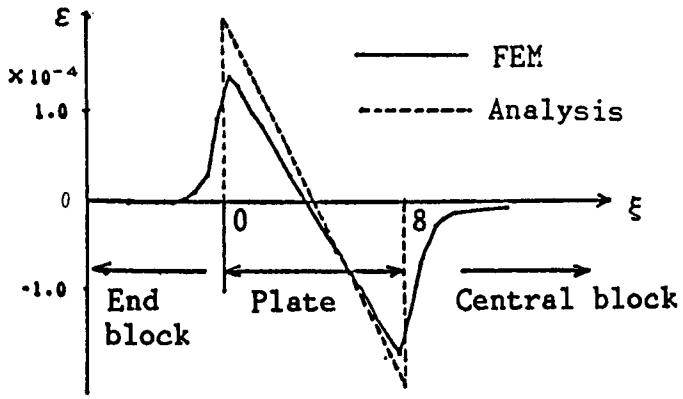

(b) $F=1.0$ kg

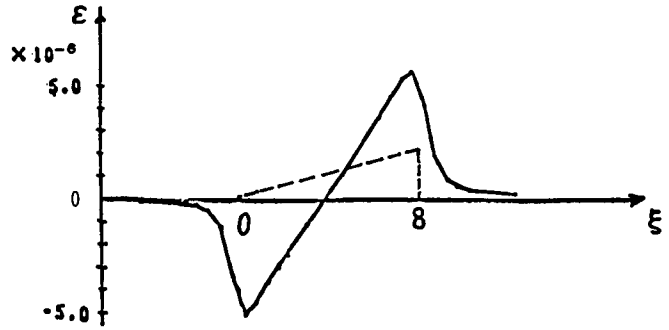

(c) $M=1.0$ kgf·mm

Fig. 15 Strain Distribution by FEM under Weak End-Block Constraint

6. Compliance Matrix

Based on the results in Sections 4 and 5, six strain gauges $S_1 \sim S_6$ have been placed at the positions shown in Fig. 16 (on the boundaries between the central block and the plates). To make the connections between the end blocks and the outer covers tighter, liquid thread lock has been used on the screws connecting them. From the measurements of these strain gauge outputs for each force component, the relation between the applied force and the resulting strain has been obtained in the form of a compliance matrix. The compliance matrix is defined by

$$\varepsilon = CF \tag{32}$$

where $F=[F_X, F_Y, F_Z, M_X, M_Y, M_Z]^T$, (kgf, kgf·m) is the force vector consisting of forces along axes X, Y, Z and moments about these axes, and $\varepsilon=[\varepsilon_1, \varepsilon_2, \cdots, \varepsilon_6]^T$ is the strains at the sensing points $S_1 \sim S_6$ caused by F. Since the desired ratio between the maximum measurable force components and moment components varies depending on applications, the force vector F is normalized as follows by an arbitrarily selected standard force unit F_N and the corresponding standard moment unit M_N, which are regarded as of the same magnitude.

$$\hat{F}=[F_X/F_N, F_Y/F_N, F_Z/F_N, M_X/M_N, M_Y/M_N, M_Z/M_N]^T \tag{33}$$

Then we obtain

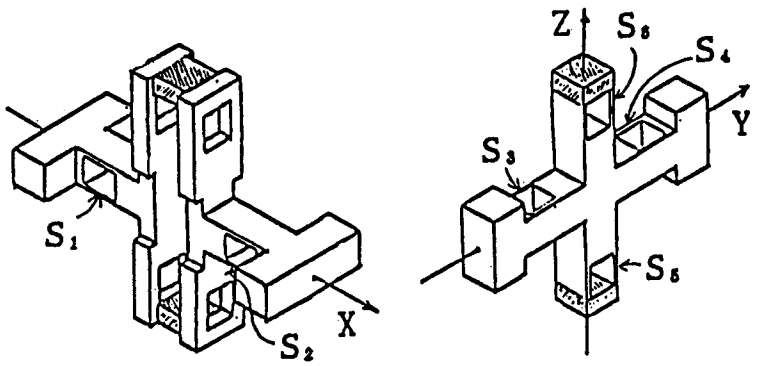

(a) PPS on X axis (b) PPS on Y and Z axes

Fig. 16 Placement of Strain Gauges $S_1 \sim S_6$

$$\varepsilon = \hat{C}\hat{F} \tag{34}$$

where $\hat{C}$ is the normalized compliance matrix given by

$$\hat{C} = C\,\mathrm{diag}[F_N, F_N, F_N, M_N, M_N, M_N] \tag{35}$$

Under an ideal situation where each sensing point responds only to the force components mentioned in section 2, C (and hence $\hat{C}$) should have the form

$$C = \begin{bmatrix} 0 & 0 & * & 0 & * & 0 \\ 0 & 0 & * & 0 & * & 0 \\ * & 0 & 0 & 0 & 0 & * \\ * & 0 & 0 & 0 & 0 & * \\ 0 & * & 0 & * & 0 & 0 \\ 0 & * & 0 & * & 0 & 0 \end{bmatrix} \tag{36}$$

where * means a non-zero value.

The compliance matrix C of the prototype sensor has been obtained as follows.

$$C \times 10^4 = \begin{bmatrix} -0.047 & 0.026 & -1.540 & 0.664 & -26.883 & -0.284 \\ 0.032 & -0.003 & -1.717 & -0.182 & 26.109 & 1.000 \\ -1.565 & -0.036 & -0.024 & 0.049 & 1.899 & 25.463 \\ -1.193 & 0.117 & -0.072 & 0.451 & -2.151 & -20.347 \\ 0.004 & 1.544 & 0.045 & 26.120 & 0.335 & -0.409 \\ 0.006 & 1.124 & -0.087 & -22.814 & -0.171 & -0.450 \end{bmatrix} \tag{37}$$

By choosing F_N and M_N as

$$F_N = 1\ (\mathrm{kgf}) \tag{38a}$$

$$M_N = 0.0587\ (\mathrm{kgf \cdot m}) \tag{38b}$$

the normalized compliance matrix is given by

$$\hat{C}\times 10^4=\begin{bmatrix} -0.047 & 0.026 & -1.540 & 0.039 & -1.578 & -0.017 \\ 0.032 & -0.003 & -1.717 & -0.011 & 1.533 & 0.060 \\ -1.565 & -0.036 & -0.024 & 0.003 & 0.111 & 1.505 \\ -1.193 & 0.117 & -0.072 & 0.026 & -0.126 & -1.194 \\ 0.004 & 1.544 & 0.045 & 1.533 & 0.020 & -0.024 \\ 0.006 & 1.124 & -0.087 & -1.339 & -0.010 & -0.026 \end{bmatrix} \tag{39}$$

The value M_N has been selected as the ratio between the average magnitude of responses for the force components and that for the moment components, i.e., letting $C=[C_{ij}]$, M_N has been given by

$$\frac{|C_{13}|+|C_{23}|+|C_{31}|+|C_{41}|+|C_{52}|+|C_{62}|}{|C_{15}|+|C_{25}|+|C_{36}|+|C_{46}|+|C_{54}|+|C_{64}|}=0.0587\,F_N \tag{40}$$

Note that the value M_E obtained from (30) and (31) as the moment which gives a strain of the same magnitude as $F_N=1$, is

$$M_E=0.104\ \text{kgf·m} \tag{41}$$

M_N given by (40) is about 56% of M_E. The reason for this difference between the analytical and measured values will probably be that the peak of the strain distribution is smaller, for the force, due to a smoothing effect, and tends to become larger than the analysis, for the moment, due the incomplete constraint of the end blocks.

The cross-coupling is now examined. Let us define a scaler α_i (i=1,2) by

$$\alpha_i=\frac{\max\{|\hat{C}_{i1}|,|\hat{C}_{i2}|,|\hat{C}_{i4}|,|\hat{C}_{i6}|\}}{\min\{|\hat{C}_{i3}|,|\hat{C}_{i5}|\}}\,, \qquad i=1,2 \tag{42}$$

Note that the elements in the numerator and the denominator correspond, respectively, to elements "0" and elements '*' in the i-th row of matrix $\hat{C}$ in (36). We also define α_i, $i=3,4,5,6$, similarly. Then α_i is a measure of

cross-coupling at the i-th sensing point. From (39) the values of α_i for the prototype sensor are obtained as

$$[\alpha_1, \alpha_2, \alpha_3, \alpha_4, \alpha_5, \alpha_6] = [0.031, 0.039, 0.074, 0.106, 0.029, 0.077] \tag{43}$$

Hence the maximum cross-coupling is 10.6% and the average is 5.9%, which are reasonably small.

One measure of uniformity of the sensor response with respect to the direction of the applied force is the condition number of $\hat{C}$ [14]. Since the singular values of $\hat{C}$ are given by {2.341, 2.233, 2.186, 2.143, 1.750, 1.638}, the condition number is 1.429. This figure is smaller than those of various force sensors discussed in ref. [14], which range from 3.16 to 15.38, meaning that the prototype sensor has a very good directional uniformity in its response.

7. Design Considerations Based on Analysis of PPS

One complaint often heard about force sensors available in the market today is that the maximum measurable moment is too small when compared with the maximum measurable force. In this section the effect of various parameters of PPS on the ratio R of force and moment which give the same strain at $\xi = l$ will be discussed based on the analysis given in Section 3. The effect of inclination of the pair of plates will also be analyzed from the viewpoint of R. Note that R has the unit of length. This ratio R would be an important index for evaluating the force sensor structure.

From (10) and (28), the ratio R is given by

$$R = \frac{3h^2l^2 + 4t^2(3d^2 + 3dl + l^2)}{2t[hl + 2t(3d + 2l)]} \tag{44}$$

Fig. 17 shows the effect of the parameters d, h, l, and t near the nominal values given in Section 4 on the ratio R. From the figure it is seen that when d and t are smaller, and when h and l are larger, the value R becomes larger. For example, if we set $t = 0.5$ and $l = 9$ instead of $t = 0.6$ and $l = 8$, while keeping h and d at their nominal values $h = 9.4$ and $d = 15$, then we have $R = 153.3$ (mm) from (44), meaning that R is increased 47% from its nominal value 104.4 (mm).

Another conceivable way of increasing R may be to modify the PPS design to the one shown in Fig. 18, in which the pairs of thin plates are not parallel. In the following we will analyze this structure and compare the value of R with that

of PPS.

The inclination of the pair is represented by the angle θ in the figure and other parameters are defined similarly to the case of PPS. We first consider the case where only a force F is applied on the center of the structure. The model is again given by Fig. 8 except that the boundary conditions now are given by

$$\xi_1 = \eta_1(l) \tan\theta \tag{45}$$

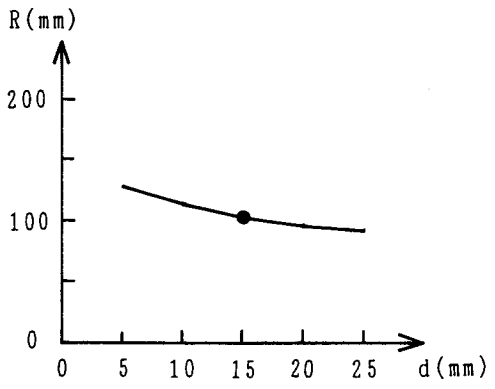

(a) Parameter d

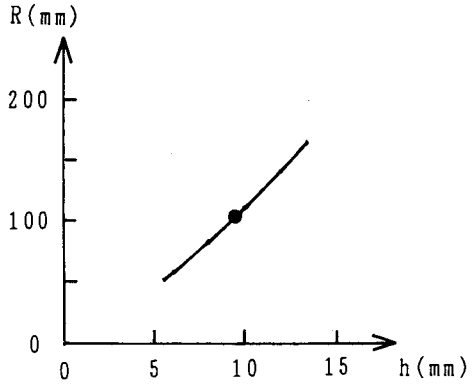

(b) Parameter h

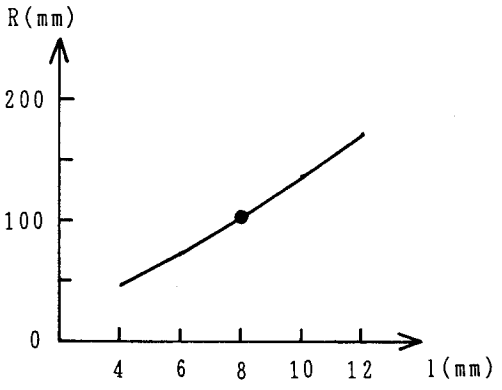

(c) Parameter l

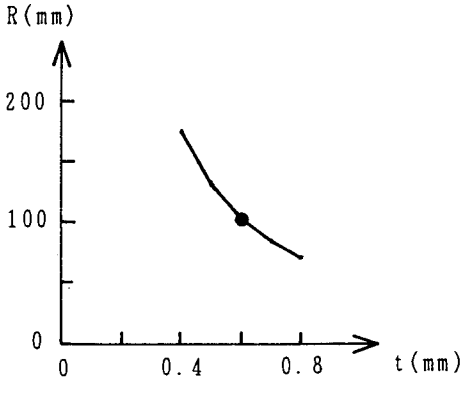

(d) Parameter t

Fig. 17 Effect of Parameters on R (–●–: Nominal point).

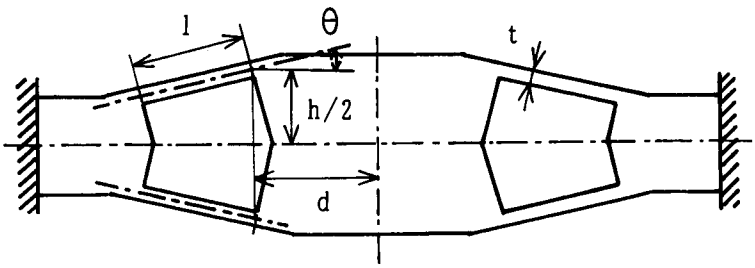

Fig. 18 Model of Inclined Plate Structure.

$$\eta_1'(l)=0 \tag{46}$$

instead of (15)–(17). Using these conditions the strain $\varepsilon_{F1}(\xi)$ on the upper surface of plate I is given by

$$\varepsilon_{F1}(\xi)=\frac{3t(2\xi-l)C_\theta+l^2S_\theta}{4Ebt(t^2C_\theta{}^2+l^2S_\theta{}^2)}F \tag{47}$$

where $S_\theta=\sin\theta$ and $C_\theta=\cos\theta$. We next consider the case where only a moment M is applied. The boundary conditions are

$$\xi_1=\alpha\sqrt{d^2+h^2/4}\sin(\phi+\theta) \tag{48}$$

$$\eta_1(l)=\alpha\sqrt{d^2+h^2/4}\cos(\phi+\theta) \tag{49}$$

and (17). After a lengthy but straightforward calculation, we obtain

$$\varepsilon_{M1}(\xi)=a_N(\xi)M/(2Ebta_D) \tag{50}$$

$$a_N(\xi)=3[l^2(hC_\theta+2dS_\theta)-tl(2l+6dC_\theta-3hS_\theta)+6t(l+2dC_\theta-hS_\theta)\xi] \tag{51}$$

$$a_D=[3(l+2dC_\theta-hS_\theta)(2dC_\theta-hS_\theta)+l(4l+6dC_\theta-3hS_\theta)]t^2+3l^2(hC_\theta+2dS_\theta)^2 \tag{52}$$

Hence we have

$$R=\frac{\varepsilon_D(lS_\theta+3tC_\theta)}{\{6[t(4l+6dC_\theta-3hS_\theta)+l(hC_\theta+2dS_\theta)]\,(t^2C_\theta{}^2+l^2S_\theta{}^2)\}} \tag{53}$$

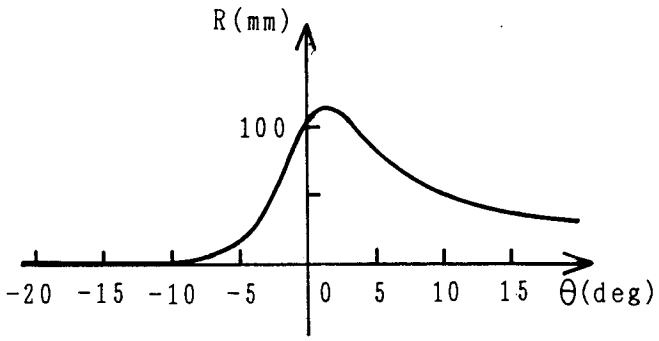

Fig. 19 Effect of θ on R

Fig. 19 shows R as a function of θ for the nominal values of other parameters. From the figure it can be seen that $\theta=0°$, which corresponds to the PPS, and is very close to the best angle θ giving the largest R.

8. Conclusion

A six-axis force sensor with a new structure, which can be called the three-dimensional cross-shape structure, has been proposed. The parallel plate structure (PPS) has been adopted as the elastic element. The force-strain relation of a PPS model has been obtained analytically by the beam theory. This result has been compared with the experimental result for a prototype sensor. It has ben shown that the prototype sensor has small cross-coupling and good directional uniformity. The validity of the three-dimensional cross-shape structure is not lost even when the PPS of the elastic elements is replaced by some other structure, for example, by a single elastic plate.

The authors would like to thank Mr. M. Kodama and Mr. M. Arao of Omron Tateishi Electronics Co. for fabricating the prototype sensor.

References

1) D.E. Whitney: Historical Perspective and State of the Art in Robot Force Control; Proc. 1985 IEEE Int. Conf. on Robotics and Automation, pp. 262–268 (1985).
2) J.K. Salisbury: Active Stiffness Control of a Manipulator in Cartesian Coordinates; Proc. 19th IEEE Conf. on Decision and Control, pp. 95–100 (1980).
3) M.H. Raibert and J.J. Craig: Hybrid Position/Force Control of Manipulators; Trans. ASME, J. DSMC, vol. 103, no. 2, pp. 126–133 (1981).

4) K. Sugimoto: Force Feedback Control of Robot Arms; J. of the Society of Instrument and Control Engineers, vol. 25, no. 1, pp. 45–50 (1986).
5) T. Yoshikawa: Dynamic Hybrid Position/Force Control of Robot Manipulators —Description of Hand Constraints and Calculation of Joint Driving Force— ; IEEE J. on Robotics and Automation, vol. RA-3, no. 5, pp. 386–392 (1987).
6) T. Yoshikawa, T. Sugie, and M. Tanaka: Dynamic Hybrid Position/Force Control of Robot Manipulators —Controller Design and Experiment— ; Proc. 1987 IEEE Int. Conf. on Robotics and Automation, pp. 2005–2010 (1987).
7) P.C. Watson and S.H. Drake: Pedestal and Wrist Force Sensors for Automatic Assembly; Proc. 5th ISIR, pp. 501–511 (1975).
8) B. Shimano: The Kinematic Design and Force Control of Computer Controlled Manipulators; Stanford Artificial Intelligence Laboratory Memo AIM-313, Mar. (1978).
9) Y. Tani, Y. Hatamura, T. Nagao, and N. Takenaka: A Study on the Dynamometer Using the Structure of Parallel Beams for Grinding; Preprints of Spring Conference of Precision Mechanics Society (1979).
10) K. Ono, Y. Hatamura, K. Ogata, R. Takada, and T. Kusaki: Development of 6 Axis Force Sensor LSA 6000; Proc. 3rd Annual Conference of Japan Robotics Socity, pp. 19–20 (1985) (in Japanese).
11) A. Yabuki and K. Asakawa: 6 Axes Force/Torque Sensors for Assembly Robots; Proc. 4th Annual Conference of Japan Robotics Society, pp. 133–134 (1986) (in Japanese).
12) G. Hirzinger and J. Dietrich: Multisensory Robots and Sensor based Path Generation; Proc. 1986 IEEE Int. Con. on Robotics and Automation, pp. 1992–2001 (1986).
13) LORD Corporation, Force/Torque Wrist Sensing Systems, 1985 (catalog).
14) M. Uchiyama, Y. Nakamura, and K. Hakomori: Evaluation of Robot Force Sensor Structure Using Singular Value Decomposition; J. of the Robotics Society of Japan, vol. 5, No. 1, pp. 4–10 (1987) (in Japanese).
15) Y. Nakamura, T. Yoshikawa, and I. Futamata: Design and Signal Processing of Six-Axis Force Sensors, Preprints of the 4th International Symposium of Robotics Research, Santa Cruz, California, Aug. 9–14 (1987).
16) Y. Ohashi: Mechanics of Material, Baihukan, Tokyo (1976) (in Japanese).